

BIO501 - Lab Immersion at Constan lab – Developmental and Cancer Cell Biology

**The role of perlecan in Activin-A mediated  
signaling in melanoma : Insights into the STING Pathway,  
Angiogenesis, and Tumor Microenvironment**

Viacheslav Bolotnikov

Contents

<b>1</b>	<b>Abstract</b>	<b>2</b>
<b>2</b>	<b>Introduction</b>	<b>2</b>
2.1	Current state of research . . . . .	2
2.2	Perspectives . . . . .	4
2.3	Project Goals and Hypotheses . . . . .	4
<b>3</b>	<b>Results</b>	<b>5</b>
3.1	Activin-A Role in Melanoma: STING Pathway Analysis . . . . .	5
3.2	Evaluating Angiogenesis and Perlecan’s Role in Melanoma . . . . .	7
3.3	Development of a Co-Culture Model . . . . .	10
<b>4</b>	<b>Discussion</b>	<b>12</b>
4.1	Activin-A Role in Melanoma: STING Pathway Analysis . . . . .	12
4.2	Evaluating Angiogenesis and Perlecan’s Role in Melanoma . . . . .	12
4.3	Development of a Co-Culture Model . . . . .	12
<b>5</b>	<b>Materials and Methods</b>	<b>13</b>
5.1	Activin-A Role in Melanoma: STING Pathway Analysis . . . . .	13
5.2	Evaluating Angiogenesis and Perlecan’s Role in Melanoma . . . . .	13
5.3	Development of a Co-Culture Model . . . . .	14
<b>6</b>	<b>Possible follow-up experiments</b>	<b>14</b>
<b>7</b>	<b>Conclusion</b>	<b>15</b>
<b>8</b>	<b>Bibliography</b>	<b>16</b>

March 19, 2025

# 1 Abstract

During my lab immersion at the Constan Lab, I aimed to investigate the roles of perlecan and Activin-A in melanoma progression by working closely with PhD student Olga Egorova. Using Western blot analyses, we quantified *Sting* levels in Activin-A over-expressing melanoma cell lines, confirming that Activin-A modulates the *Sting* pathway. Immunofluorescence studies on cryosections and formalin-fixed paraffin-embedded (FFPE) sections allowed us to identify the appropriate antibody for detecting whether Activin-A promotes angiogenesis by depleting pericytes. This finding is critical for understanding tumor growth and sets the stage for future experiments. Additionally, we began developing a 3-D extracellular matrix model to study the influence of perlecan and Activin-A on melanoma progression. These findings highlight the pivotal roles of Activin-A and perlecan in melanoma and set the stage for future research to develop targeted therapies for this aggressive cancer.

## 2 Introduction

Melanoma, a malignant tumor of melanocytes, is one of the most aggressive forms of skin cancer. Its ability to metastasize rapidly makes it a significant cause of cancer-related mortality. Understanding the molecular mechanisms that drive melanoma progression and resistance to therapy is crucial for developing effective treatments. One of the molecules of interest in this context is Activin-A, a member of the TGF- $\beta$  superfamily, known for its roles in regulating various cellular processes, including proliferation, differentiation, and immune responses (*Donoval et al. (2017)* [1]) (*Pinjusic et al. (2024)* [11]). This report explores the role of Activin-A in melanoma, particularly focusing on the examination of changes in *Sting* pathway, angiogenesis, and the development of a 3-D co-culture model to further investigate the interactions between tumor cells and endothelial cells within the tumor microenvironment.

### 2.1 Current state of research

#### Extracellular matrix proteins and melanoma

##### Activin-A

*Donovan et al. (2017)* [1] demonstrated that paracrine signaling of Activin-A promotes melanoma growth and metastasis by enhancing the invasive capabilities of melanoma cells and supporting the formation of a pro-tumorigenic microenvironment. This study highlights that melanoma cells secrete Activin-A, which activates signaling pathways contributing to increased tumor aggressiveness and metastatic potential. Additionally, *Murphy et al. (2023)* [10] found that Activin-A-mediated polarization of cancer-associated fibroblasts and macrophages confers resistance to checkpoint immunotherapy in melanoma by creating an immunosuppressive microenvironment. These findings underscore the importance of targeting Activin-A signaling in therapeutic strategies aimed at controlling melanoma progression.

## **Perlecan**

Perlecan, a heparan sulfate proteoglycan, plays a crucial role in the tumor micro-environment by regulating cell proliferation, migration, and angiogenesis. *Li et al. (2010)* [5] found that Activin-A binds to perlecan through its pro-region, which contains heparan sulfate binding sites. This interaction is significant for the localization and availability of Activin-A within the tumor micro-environment, influencing angiogenic processes and potentially facilitating melanoma progression.

## **Biological mechanism in melanoma**

### **STING Pathway**

The STING (Stimulator of Interferon Genes) pathway is a critical component of the innate immune response, particularly in the detection of cytosolic DNA from pathogens and damaged cells. Activation of *Sting* leads to the production of type I interferons and other cytokines, essential for mounting an effective immune response against tumors (*Woo et al. 2014*) [12].

The study by *Pinjusic et al. (2024)* [11] revealed that Activin-A secreted by melanoma cells can modulate the immune response by interfering with the *Sting* and *JAK-STAT* pathways. Specifically, when Activin-A is knockdown from YUMM 3.3 tumors, the control tumor size remains stable, whereas in YUMM 3.3- $\beta$ A (Activin-A over-expressing tumor model) the tumor size decrease significantly, underlying a *Sting* dependence.

### **Angiogenesis**

In endothelial cells, activin-a has been associated with both angiogenic and anti-tumorigenic effects.

*Kaneda et al. (2011)* [3] was among the first to state that Activin-A is directly implicated in inhibiting cell proliferation. *Maeshima et al. (2004)* [6] however have demonstrated the possible angiogenic effect of activin-a by promoting *VEGF-A* expression. Lately, *Pinjusic et al. (2024)* [11], found that Activin-A almost completely depleted pericytes, which are crucial for the maturation and function of microvessels. The absence of pericytes might influence tumor vascularization and the stability of newly formed blood vessels. However blood vessel leakiness in tumors is associated with increased cancer growth and predisposition to metastasis (*McDonald et al. 2002*)[8].

This suggests a complex role in angiogenesis that may vary between different tumor types.

## **Co-Culture Models in Cancer Research**

Co-culture models are essential tools in cancer research as they allow the study of interactions between different cell types in the tumor microenvironment. These models can mimic the complex cellular interactions that occur *in vivo*, providing insights into tumor biology, drug responses, and mechanisms of resistance.

It is now known that extracellular matrix in aggressive melanomas contributes to tumor cell morphogenesis, modulates interactions between tumor cells and endothelial cells, and may contribute to an extra-vascular matrix-directed circulation (*Maniotis et al. (2002)*) [7]. Thus in order to be accurate in our studies and study the real impact of

ECM proteins like perlecan, we need to recreate and co culture our cells in a extracellular matrix. In order to do that, some protocols like the one published by *Franco-Barraza et al. (2016)* [2] are available and allow to grow extracellular matrix from fibroblasts.

## 2.2 Perspectives

Significant progress has been made in understanding the molecular mechanisms driving melanoma progression, particularly the roles of Activin-A, *Sting*, and the tumor microenvironment. Activin-A has been shown to promote melanoma growth and metastasis by enhancing invasive capabilities and creating a pro-tumorigenic microenvironment. It modulates the *Sting* and *JAK-STAT* pathways, leading to immune evasion and reduced effectiveness of anti-tumor responses. The complex interactions between Activin-A and endothelial cells further highlight the intricate role of angiogenesis in melanoma progression.

However, there remains a critical gap in understanding the full extent of these interactions and their implications for therapeutic strategies. Especially because a lot of these mechanisms can be model specific or broad and they also have not been associated with observational changes in tumor size yet. Our study aims to address this by investigating the impact of Activin-A on the *Sting* pathway and angiogenesis using if possible advanced co-culture models. By recreating the tumor microenvironment and studying the interactions between melanoma cells, endothelial cells, and fibroblasts, we hope to uncover new insights into how Activin-A drives tumor growth and immune evasion.

## 2.3 Project Goals and Hypotheses

The goal of this project is to elucidate the role of Perlecan and Activin-A in melanoma progression, specifically focusing on their influence on the *Sting* pathway, angiogenesis, and the tumor microenvironment. Our hypotheses are that Activin-A overexpression in melanoma cells modulates the *Sting* pathway to promote immune evasion, that Perlecan depletion disrupts angiogenesis and vascular stability, and that a 3-D co-culture model can effectively simulate the tumor microenvironment to study these interactions. By employing a combination of Western blotting, immunofluorescence, and advanced cell culture techniques, we aim to uncover the molecular mechanisms by which Perlecan and Activin-A contribute to melanoma growth and metastasis, ultimately identifying potential therapeutic targets.

## 3 Results

### 3.1 Activin-A Role in Melanoma: STING Pathway Analysis

In a recent study, *Pinjusic et al. (2024)* demonstrated that in YUMM 3.3 cells, shRNA targeting *STING* led to a significant reduction in tumor size in  $\beta$ A tumors but had no effect on control tumors, indicating that YUMM 3.3 -  $\beta$ A depends on *STING*. This observation prompts the question whether a similar trend occurs in the B16F1 cell line and if *STING* is more expressed in B16F1 -  $\beta$ A (Activin-A over-expression) compared to controls.

Moreover, in previous experiment, we noticed that B16F1-ctl shScrambled and B16F1- $\beta$ A shScrambled grow at the same size, which is intriguing given that Activin-A, known for promoting tumor growth, did not differentiate tumor size between the two conditions. This suggests that even scrambled shRNA may be detected by the *STING* pathway as foreign genetic material, particularly if *STING* is more expressed in the  $\beta$ A line, potentially explaining the absence of difference in tumor sizes.

Our study aims to further investigate the role of Activin-A in melanoma, specifically focusing on its impact on the *STING* pathway. Utilizing murine melanoma cell lines with varying levels of Activin-A expression, we probed for total and phosphorylated *STING* (t*STING* and p*STING*) to understand how Activin-A influences *STING* pathway activation. This will help gain deeper insights into the mechanisms of immune evasion and identify potential therapeutic targets to enhance anti-tumor immunity.

#### Total STING (t*STING*) Expression

Western blot analysis revealed that the expression levels of *tSTING* was moderately increased in the B16F1- $\beta$ A cell lines compared to the control lines. Notably, there was no significant difference in *tSTING* levels between the scrambled and parental controls for both the control and Activin-A overexpressing lines (Figure 1).

#### Total STING (t*STING*) Expression in Confluent Cells

Interestingly, when cells were cultured to confluence, Western blot analysis showed higher levels of *tSTING* in the control cell lines compared to the Activin-A overexpressing lines (Figure 2).

#### Phosphorylated STING (p*STING*) Expression

Attempts to probe for *pSTING* did not yield sufficient signal despite trying two different antibodies, indicating that the Western blot was not sensitive enough under the conditions used to detect *pSTING*. Further optimization and additional stimuli may be required to obtain clear results for *pSTING* (data not shown).

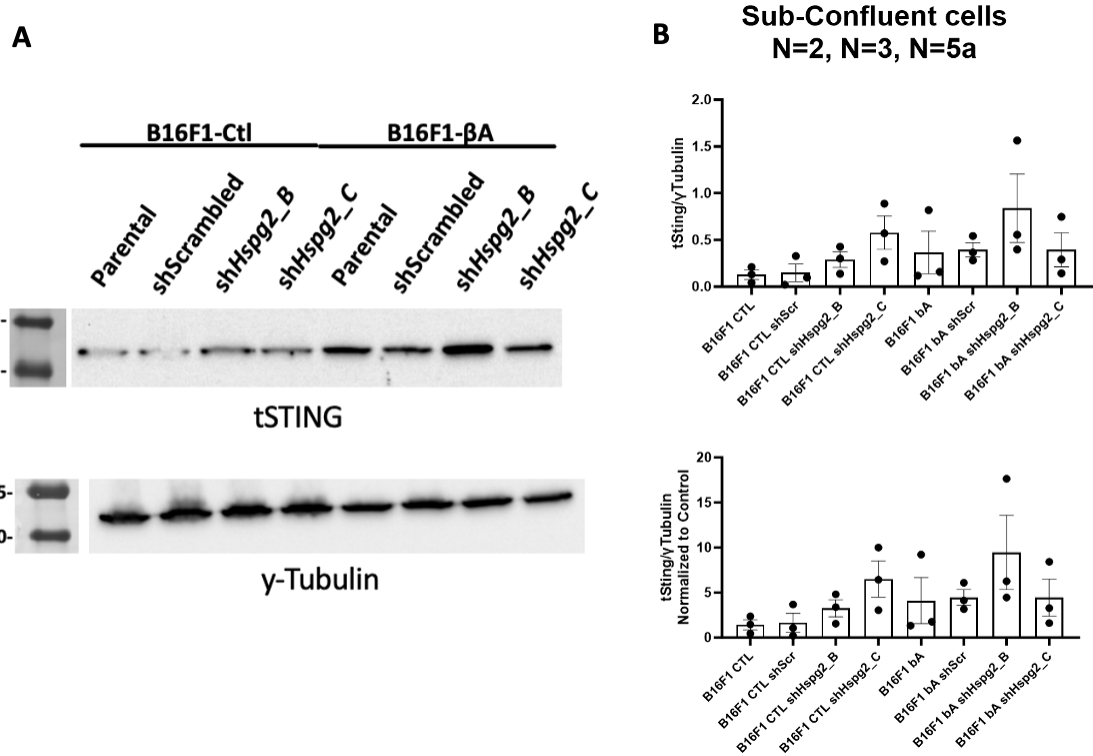


**Figure 1: Analysis Total STING (tSTING) expression in B16F1 cell lines.**  
**A.** Western blot analysis of tSTING and  $\gamma$ -tubulin (loading control) after native SDS-PAGE of cell supernatant from one representative experiment out of 3. Full-length protein (predicted MW 42 kDa). Protein size markers are indicated to the left. **B.** Data represents expression means of 3 independent experiments  $\pm$  SEM.

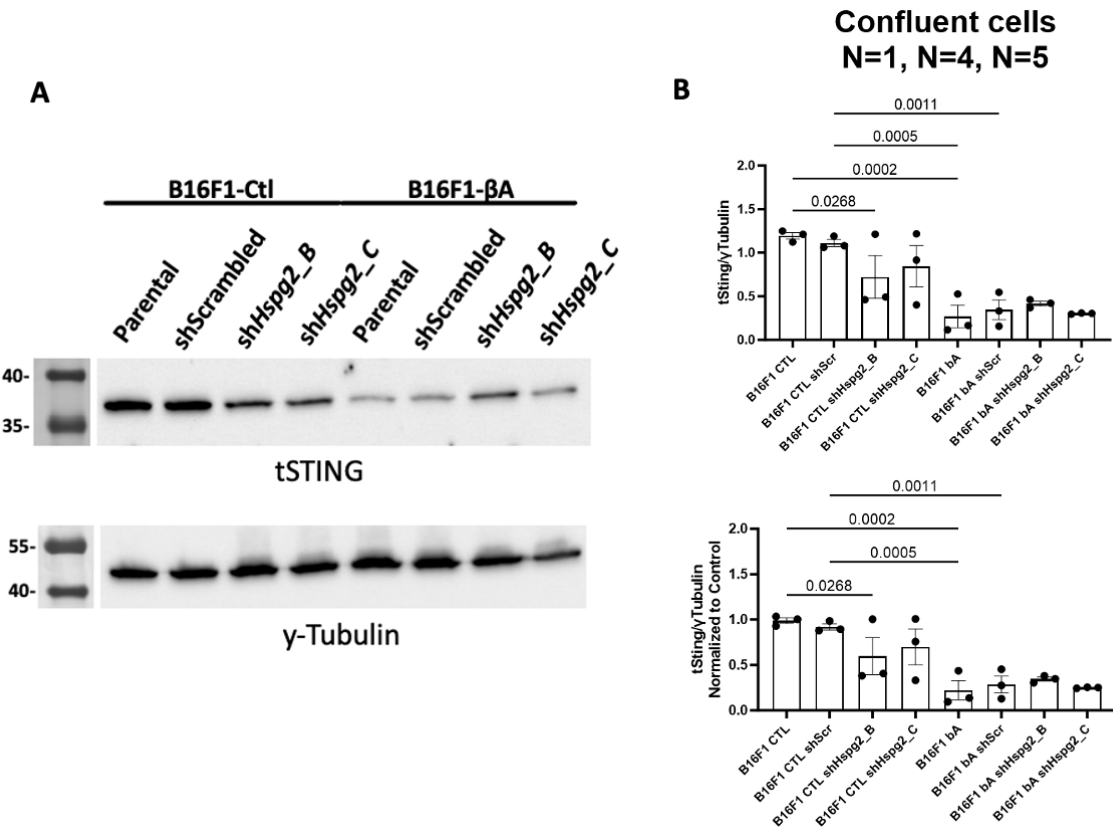


**Figure 2: Analysis Total STING (tSTING) expression in B16F1 over confluent cell lines.** **A.** Western blot analysis of tSTING and  $\gamma$ -tubulin (loading control) after native SDS-PAGE of cell supernatant from one representative experiment out of 3. Full-length protein (predicted MW 42 kDa). Protein size markers are indicated to the left. **B.** Data represents expression means of 3 independent experiments  $\pm$  SEM.

### 3.2 Evaluating Angiogenesis and Perlecan's Role in Melanoma

To investigate the role of perlecan and angiogenesis in melanoma, we conducted an immunofluorescence study on cryosections and formalin-fixed paraffin-embedded (FFPE) sections of murine melanoma samples. The samples included both control and Activin-A overexpressing cell lines. Our goal was to identify the appropriate antibodies for detecting pericytes, endothelial cells, and other relevant markers to enable detailed future studies on angiogenesis and vascular stability in melanoma.

#### Immunofluorescence Results

Initially, in cryosections, anti-NG2 was used to detect pericytes, but it did not yield satisfactory results (Figure 3). Subsequently, anti-PDGFR $\beta$  was employed, which provided better detection of pericytes (Figure 4). Thus anti-PDGFR $\beta$  was employed in FFPE sections to detect pericytes, but it did not yield satisfactory results (Figure 5).

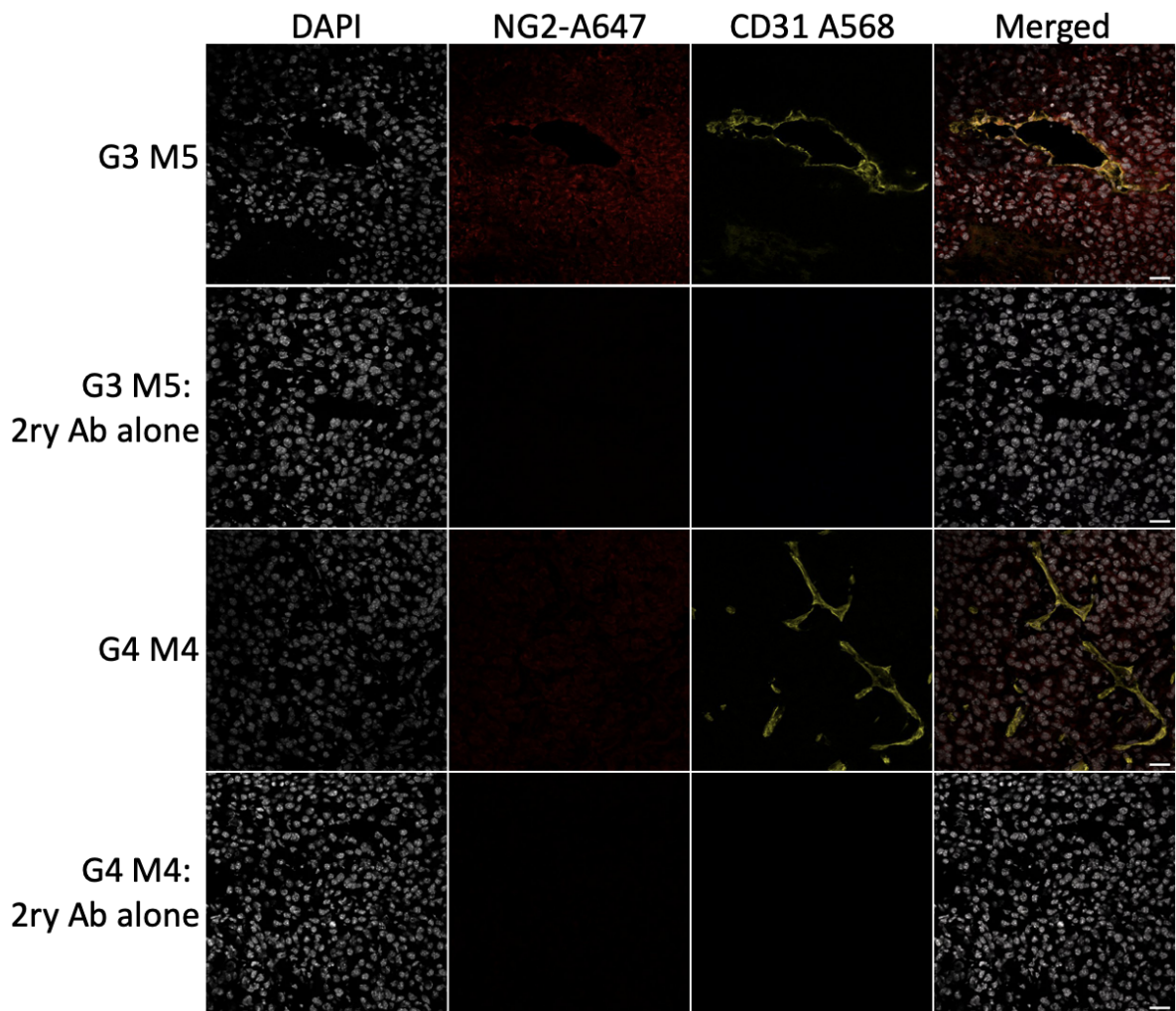


**Figure 3: Expression of NG2 and CD31 in Control and Activin-A Overexpressing Melanoma Murine Samples.** Immunofluorescence staining of cryosections from OE-02 Group 3 and Group 4 mice. NG2 (red) and CD31 (yellow) are shown with DAPI nuclear staining (grey). Panels include B16F1-Ctl and B16F1- $\beta$ A Amoxicillin groups, with and without secondary antibodies. Images were captured at 40X magnification.

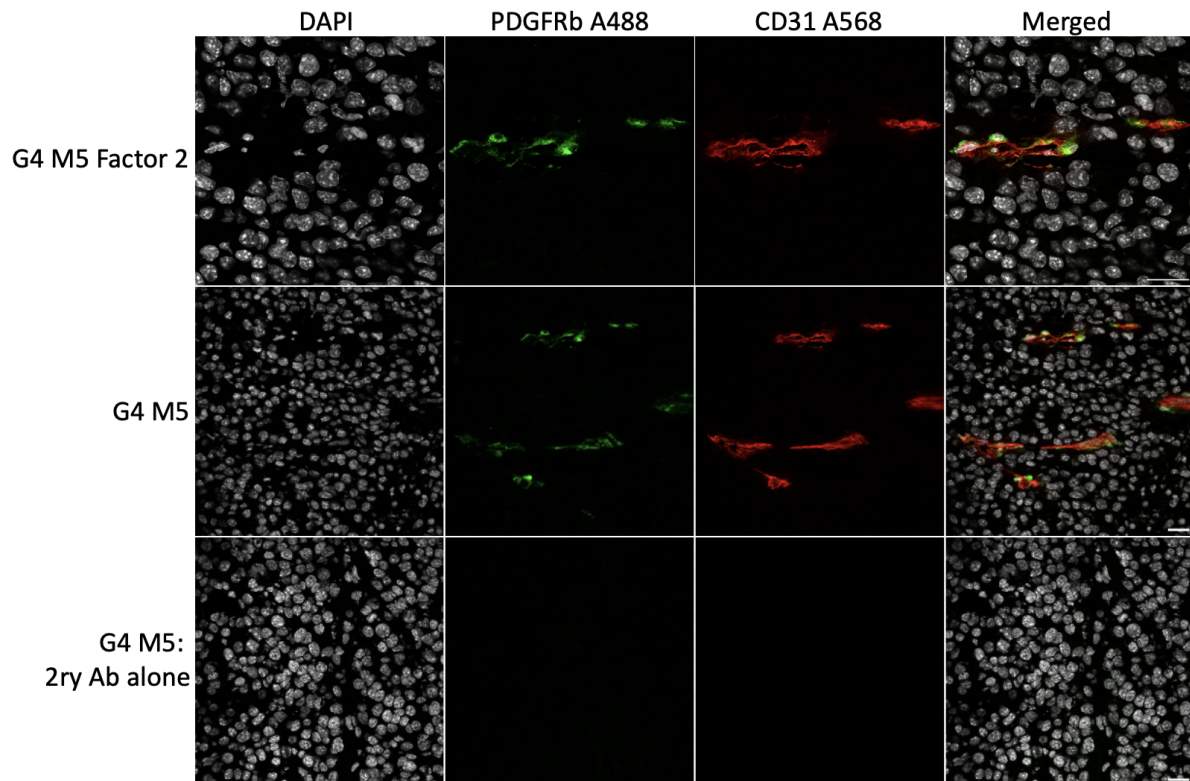


**Figure 4: Expression of PDGFR $\beta$  and CD31 in Control and Activin-A Overexpressing Melanoma Murine Samples.** Immunofluorescence staining of cryosections from OE-02 Group 4 mice. PDGFR $\beta$  (green) and CD31 (red) are shown with DAPI nuclear staining (grey). Panels include B16F1- $\beta$ A Amoxicillin group, with and without secondary antibodies. Images were captured at 40X magnification.

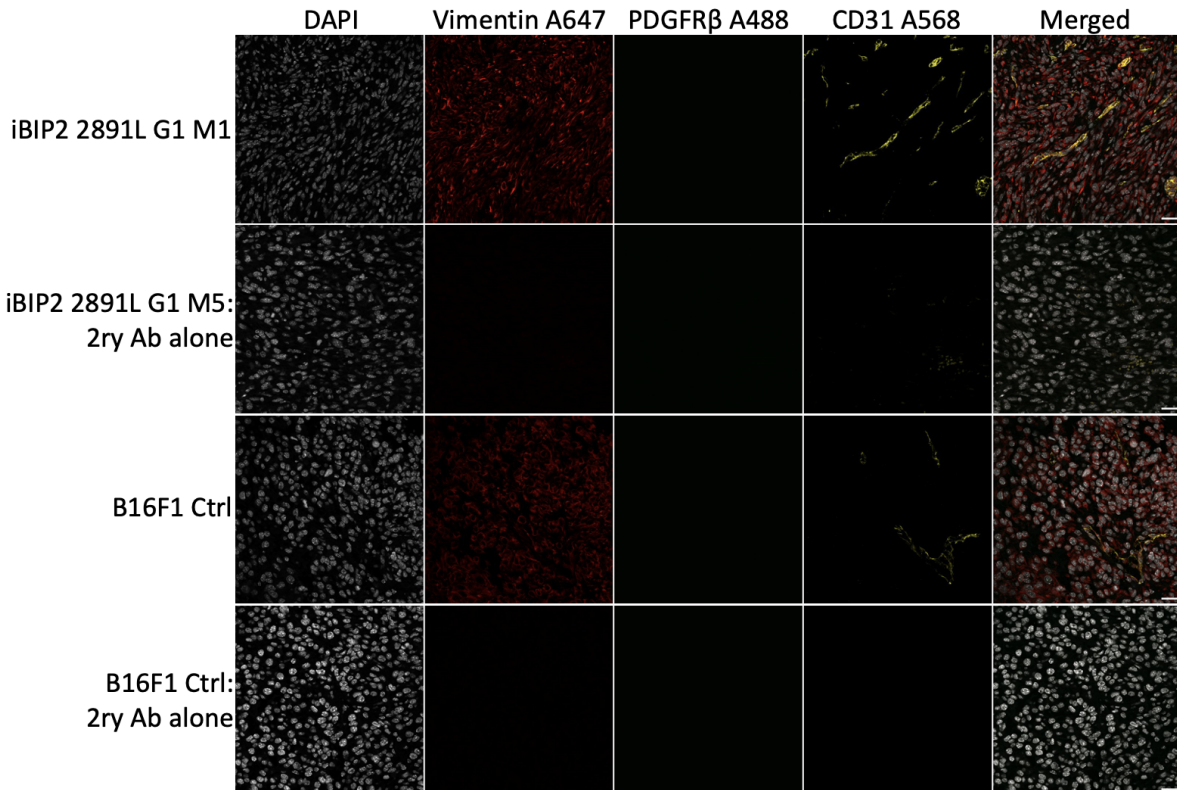


**Figure 5: Expression of Vimentin, PDGFR $\beta$ , and CD31 in Formalin-Fixed Paraffin-Embedded (FFPE) sections of Melanoma Murine Samples.** Immunofluorescence staining of paraffin sections from B16F1 Ctrl and iBIP2 2891L G1 samples. Vimentin (red), PDGFR $\beta$  (green), and CD31 (yellow) are shown with DAPI nuclear staining (grey). Panels include iBIP2 2891L G1 and B16F1 Ctrl samples, with and without secondary antibodies. Images were captured at 40X magnification.

### 3.3 Development of a Co-Culture Model

The goal of this experiment was to develop an *in vitro* 3-D tumor cell/endothelial cell co-culture system to explore the role of Perlecan in the modulation of Activin-A signaling. We used NIH-3T3 mouse fibroblast cell lines. These fibroblast cells were genetically modified to knock out the production of perlecan and Activin-A, which, while slightly reducing the physiological accuracy of the model, allowed us to isolate the effects of perlecan and Activin-A produced by cancer cells alone. This approach aimed to create a more controlled environment to study the influence of these factors from cancer cells on the tumor microenvironment. The cell lines tested included NIH3T3 sh*Inhba*\_C2 with additional depletion of perlecan targeting regions B and C, as well as control lines.

### Protein Extraction and Western Blot Analysis

Protein extraction and Western blot analysis were performed to quantify the levels of perlecan and Activin-A in the modified cell lines. The results demonstrated varying degrees of perlecan depletion across the different cell lines.

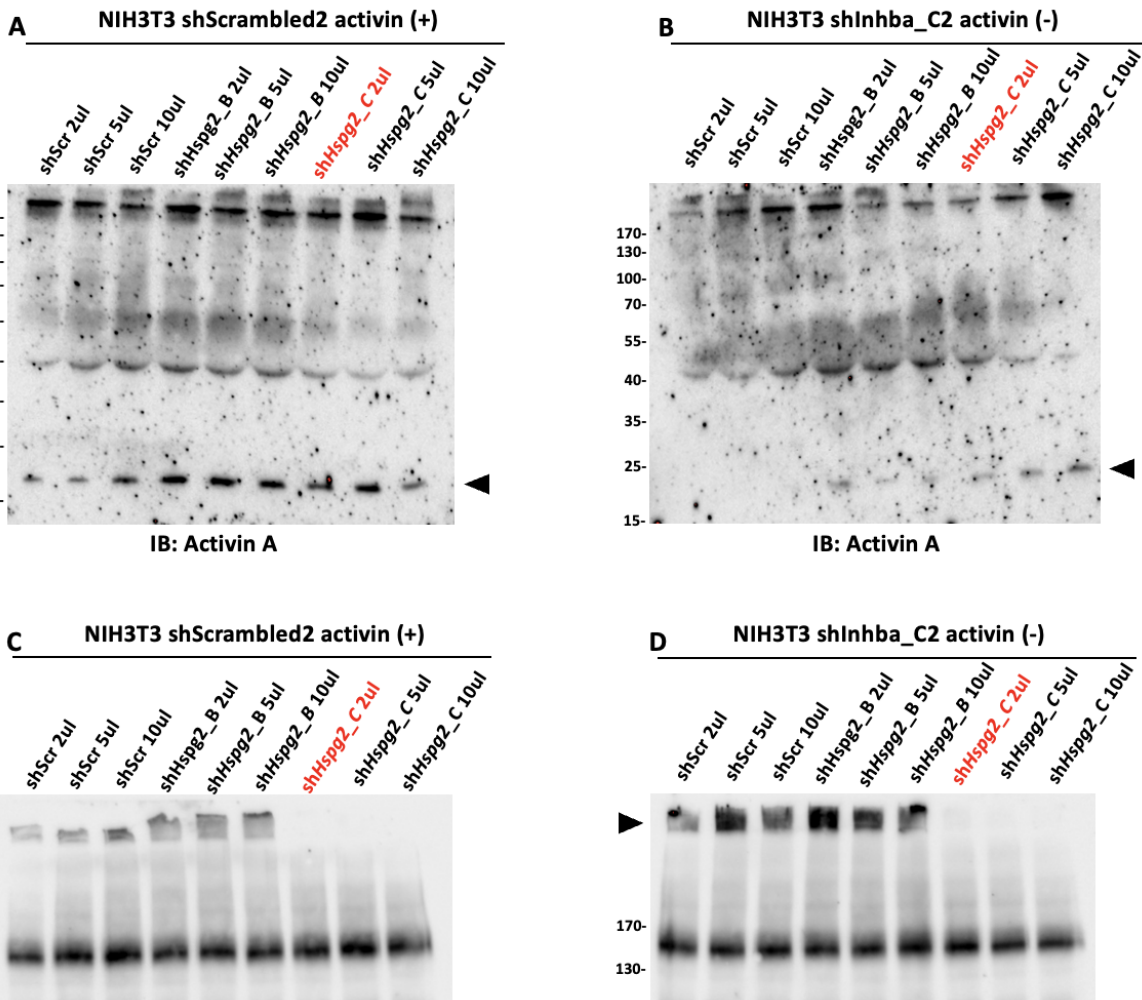


**Figure 6: Validation of siRNA-mediated downregulation of Perlecan and Activin-A expression in different NIH3T3 cell lines.** **A. B.** Western blot analysis of Activin after native SDS-PAGE of cell supernatant from one representative experiment out of three. Arrow: full-length protein (predicted MW 20 kDa). Protein size markers are indicated to the left. **C. D.** Western blot analysis of Perlecan after native SDS-PAGE of cell supernatant from one representative experiment out of two. Arrow: full-length protein (predicted MW 467 kDa). Protein size markers are indicated to the left.

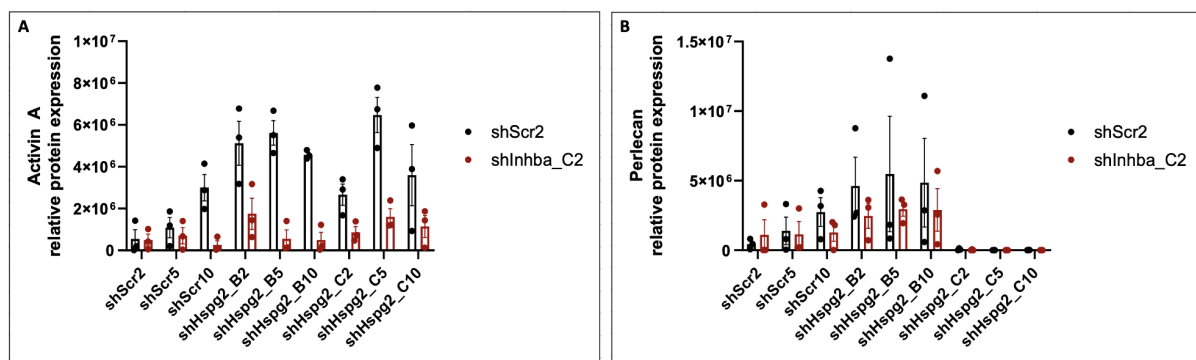


**Figure 7: Western blot quantification of perlecan and Activin-A levels in NIH3T3 fibroblast cell lines.** **A.** The bar graph shows adjusted total band volume (intensity) for perlecan. **B.** The bar graph shows adjusted total band volume (intensity) for activin. The cell lines include both NIH3T3 shInhba\_C2 and NIH3T3 shScr2, with varying volumes of lentivirus used for knockdown (2, 5, 10 μL) targeting regions B and C of perlecan. Data represent means of three independent experiments ± SEM.

## 4 Discussion

### 4.1 Activin-A Role in Melanoma: STING Pathway Analysis

The main purpose of this experiment was to ensure that the shScrambled (shScr) line was similar to the parental one, confirming that our knockdown strategy did not affect other aspects of the cancer cells. This was successfully proven, and we also confirmed the findings of *Pinjusic et al. (2024)* [11], demonstrating *tSTING* was more present in the Activin-A overexpressing cancer cell lines.

Additionally, this experiment revealed that cell confluency has a significant impact on *Sting* production. In over-confluent conditions, the control cell line exhibited a marked increase in STING production, rising from baseline levels to 2-fold higher, whereas the Activin-A overexpressing cell lines maintained a stable level of 0.5 ratio of tSTING/ $\gamma$ -Tubulin. This indicates that Activin-A overexpressing cell lines may induce additional signals upon reaching confluence that regulate the production or secretion of *Sting*. We could not find anything in the literature that was highlighting this density parameter when culturing B16F1 cell lines or any related *Sting* contact inhibition. Actually, one paper from *Lee et al. 2022* [4] showed that YAP inhibits HCMV replication by impairing *Sting*-mediated nuclear transport. This suggests a potential interaction between the *Sting* pathway and the *Hippo-YAP* signaling pathway, which is known to be related to cell density.

Although probing for *pSTING* did not yield successful results due to insufficient signal, this highlights the need for further optimization of the protocol. Successful detection of *pSTING* in future experiments would provide additional valuable information regarding the activation state of the *Sting* pathway in these cell lines.

### 4.2 Evaluating Angiogenesis and Perlecan’s Role in Melanoma

These immunofluorescence experiments demonstrated that anti-PDGFR $\beta$  A488 effectively detected pericytes in our cryosections (Figure 4) compared to anti-NG2 A467 (Figure 3). Consequently, this antibody will be employed in a more extensive analysis to determine if our hypothesis that pericytes are significantly depleted in activin-A overexpressing tumors is true. However this antibody didn’t work on FFPE sections (Figure 5). It would be interesting to try anti-NG2 on FFPE sections, otherwise we should look in the literature for other antibodies.

### 4.3 Development of a Co-Culture Model

The various Western blot analyses allowed us to identify the NIH3T3 sh*Inhba*\_C2 + sh*Hspg2*\_C2 fibroblast cell line as the optimal choice for growing the 3D extracellular matrix. This cell line yielded the best results for depleting pericytes and activin-A (Figure 6, 7), thereby minimizing confounding factors when studying cancer cells. However, the high levels of perlecan under sh*Hspg2*\_B lentivirus transduction is surprising and we could not find any explication yet. Currently, we are implementing and refining the procedure outlined by *Franco-Barraza et al. (2016)* [2] to achieve the desired matrix. The next step

involves quantifying the nature and amount of proteins in the grown matrix, after which we will commence the co-culture experiments.

## 5 Materials and Methods

### 5.1 Activin-A Role in Melanoma: STING Pathway Analysis

To investigate the role of Activin-A in *Sting* pathway activation, we utilized murine melanoma cell lines with varying levels of Activin-A expression and perlecan depletion. The cell lines used included control lines (B16F1-Ctl Parental, B16F1-Ctl shScrambled, B16F1-Ctl sh*Hspg2-B*, and B16F1-Ctl sh*Hspg2-C*) and Activin-A overexpressing lines (B16F1- $\beta$ A Parental, B16F1- $\beta$ A shScrambled, B16F1- $\beta$ A sh*Hspg2-B*, and B16F1- $\beta$ A sh*Hspg2-C*). Perlecan depletion was achieved using shRNA targeting *Hspg2*, with two distinct regions (HB and HC) deleted.

Western blot analysis was performed using specific antibodies. The primary antibodies used were *Sting* (D2P2F) Rabbit mAb (Cell Signaling C/N13647) incubated at 4°C overnight, Phospho-STING (Ser365) (D8F4W) Rabbit mAb (Cell Signaling C/N72971) incubated at 4°C overnight, and  $\gamma$ -Tubulin for loading control incubated at 4°C overnight. The secondary antibodies used were Anti-Rabbit HRP for the STING and Phospho-STING antibodies, and Anti-Mouse HRP for the  $\gamma$ -Tubulin, all incubated for 1 hour at room temperature.

Cells were cultured under standard conditions and treated as necessary to maintain overexpression of Activin-A or perlecan depletion. Proteins were extracted using RIPA buffer supplemented with protease and phosphatase inhibitors, and protein concentrations were determined using a BCA assay to ensure equal loading. Each sample loaded contained 100 $\mu$ g of protein in a 30 $\mu$ L volume. Proteins were separated by SDS-PAGE and transferred onto nitrocellulose membranes. The membranes were blocked and incubated with primary antibodies, followed by HRP-conjugated secondary antibodies. Detection was performed using chemiluminescence.

### 5.2 Evaluating Angiogenesis and Perlecan's Role in Melanoma

To investigate the role of perlecan and angiogenesis in melanoma, we conducted an immunofluorescence study on cryosections and paraffin-embedded sections of murine melanoma samples. The cell lines used for cryosections included control lines (OE-02 Group 3: B16F1-Ctl Amoxicillin Mouse 5) and Activin-A overexpressing lines (OE-02 Group 4: B16F1- $\beta$ A Amoxicillin Mouse 4). The cell lines used for paraffin-embedded sections included B16F1 Ctrl and iBIP2 2891L G1.

The primary antibodies used for staining were Rat anti-PDGFR $\beta$  (eBioscience 14-1402-82, dilution 1:100) for the detection of pericytes, Goat anti-CD31 (R&D AF3628, dilution 1:100) for the detection of endothelial cells, AF647 anti-NG2 (Santa Cruz sc-53389, dilution 1:100) also for the detection of pericytes, and Rabbit anti-Vimentin (Cell Signaling 5741S, dilution 1:100) for the detection of cancer cells. The primary antibodies were incubated at 4°C overnight.

The secondary antibodies used were Donkey anti-Rat A488 (dilution 1:800), Donkey

anti-Goat A568 (dilution 1:800), and Donkey anti-Rabbit A647 (dilution 1:800), all incubated for 1 hour at room temperature. Nuclear staining was performed using DAPI at a dilution of 1:5000 for cryosections and 1:10000 for paraffin sections.

All images were captured at 40X magnification.

The cryosections and paraffin sections were incubated, treated, and mounted using standard protocols commonly used in immunofluorescence studies, ensuring consistent and reproducible results.

### 5.3 Development of a Co-Culture Model

We selected NIH 3T3 cells for our study due to their ease of handling in laboratory settings and because they are widely cited in the scientific literature. Moreover, the protocol described by *Franco-Barraza et al. (2016)*[2], which we are using, is specifically optimized for them. Initially, we used NIH3T3 cell lines with efficient Activin-A depletion, designated as NIH3T3 shInhba\_C2 (where "C" refers to the targeted region and "2" indicates the volume of lentivirus used for transduction). Control cells were designated as NIH3T3 shScr2, where "scr" denotes a scrambled shRNA sequence used as a control. Both NIH3T3 shInhba\_C2 and NIH3T3 shScr2 cell lines exhibited resistance to neomycin, which was used for selection.

To further generate NIH3T3 cell lines with additional depletion of perlecan, various combinations of lentivirus volumes (2, 5, 10  $\mu$ L) and targeted regions (B and C) were tested. The shRNA used are named shHspg2\_B/C. The efficiency of perlecan depletion was assessed through protein extraction and Western blot analysis. Cell lysates were collected and subjected to acetone precipitation for lysis, with a non-reducing agent used to maintain Activin-A in its dimeric form. The lysates were run on 6% 1.5 mm gels for perlecan detection and on 10% 1.5 mm gels for Activin-A detection.

Proteins were transferred to membranes and probed with specific antibodies to quantify the levels of perlecan and Activin-A. The primary antibodies used were Biotinylated Activin A antibody (R&D, 1:500) detected with Streptavidin-HRP (1:1000) for Activin-A, and Perlecan antibody (Santa Cruz, 1:500) detected with HRP-conjugated secondary antibody (1:1000) for perlecan.

## 6 Possible follow-up experiments

The next experiment already planned will use the NIH3T3 modified cell lines to produce a robust 3-D extracellular matrix and to co-culture cancer and endothelial cells. It will allow to study the phosphorylation of *Smad2* into *pSmad2* in endothelial cells by immunofluorescence in the presence/absence of perlecan in the cancer cells allowing for precise and accurate studies on the impact of perlecan and Activin-A on melanoma progression. The methodology for producing ECM proteins and subsequent analyses will be adapted from *Franco-Barraza et al. 2016* [2], and the experimental setup will be based on protocols described by *Murphy et al. 2022* [9] 8.

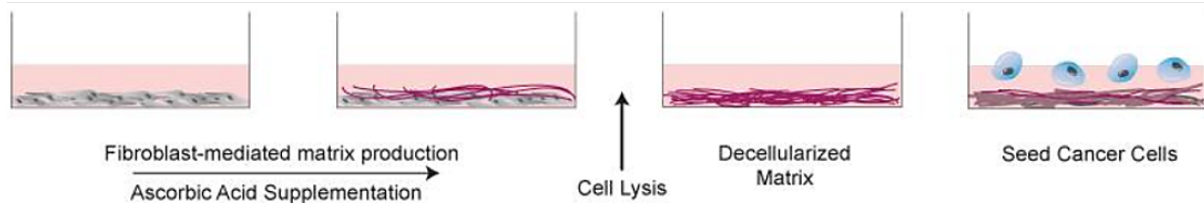


**Figure 8:** Adapted from *Murphy et al. 2022*

However, during my lab immersion, I considered two additional experiments:

Firstly, as discussed in a lab meeting, collagen type IV is a strong indicator of blood vessel leakiness and is produced by pericytes. To investigate whether pericyte depletion in Activin-A overexpressing melanoma reduces blood vessel stability due to decreased collagen type IV production, I propose immunostaining for pericytes and collagen type IV in melanoma cell lines with and without Activin-A overexpression. We will also assess vascular permeability and attempt to detect fibrinogen as a marker of damaged blood vessels. We expect reduced pericyte numbers and collagen type IV levels in Activin-A overexpressing tumors, correlating with increased vascular leakiness. This study aims to elucidate the role of pericytes and collagen type IV in maintaining vascular stability in melanoma.

Secondly, we observed that cell confluency affects *Sting* production, with control cells showing a 2-fold increase under over-confluent conditions, while Activin-A overexpressing cells remained stable. To investigate this further, I propose growing B16F1 control and Activin-A overexpressing cell lines at varying confluence levels (low, medium, high), quantifying *Sting* levels using Western blotting, assessing activation of *Sting* related pathway and density activation pathway like *Hippo-YAP* through immunoblotting or immunofluorescence. This study aims to uncover the mechanisms regulating *Sting* production in response to contact.

## 7 Conclusion

In summary, our findings reinforce the role of Activin-A in modulating the STING pathway in melanoma, highlighting its contribution to immune evasion. The experiments demonstrated that Activin-A overexpression leads to increased total STING levels, and the importance of cell confluency was underscored as a crucial factor in these analyses. Future studies should focus on optimizing the detection of phosphorylated STING (pSTING) to gain deeper insights into the signaling mechanisms involved. Additionally, our immunofluorescence studies revealed that we have identified efficient antibodies that will facilitate future investigations into whether Activin-A indeed depletes pericytes in B16F1 cell lines. Finally, the development of a 3-D co-culture model using genetically modified fibroblasts provided a robust platform to study the interactions between Perlecan and Activin-A. We now have an optimal cell line to create a 3-D matrix, allowing for deeper exploration of the impact of Perlecan on cancer and endothelial cells.

## Acknowledgment

The author would like to thank PhD student Olga Egorova for her assistance during this semester, Professor Daniel B. Constam for his trust and for offering this opportunity,

and all the other members of the lab who provided valuable advice and help. This work was supported by the Swiss National Science Foundation (SNSF) and OncoSuisse (funding agencies) and in part by using the resources and services of the Constam Lab, the Histology Facility, and the Research Core Facility at the School of Life Sciences of EPFL.

## 8 Bibliography

- [1] P. Donovan, O. Dubey, Susanna E. Kallioinen, Katherine W. Rogers, K. Muehlethaler, Patrick Müller, D. Rimoldi, and D. Constam. Paracrine activin-a signaling promotes melanoma growth and metastasis through immune evasion. *bioRxiv*, 2017.
- [2] J. Franco-Barraza, D.A. Beacham, M.D. Amatangelo, and E. Cukierman. Preparation of extracellular matrices produced by cultured and primary fibroblasts. *Current Protocols in Cell Biology*, 71:10.9.1–10.9.34, Jun 2016.
- [3] H. Kaneda, T. Arao, K. Matsumoto, M. A. De Velasco, D. Tamura, K. Aomatsu, and et al. Activin a inhibits vascular endothelial cell growth and suppresses tumour angiogenesis in gastric cancer. *British Journal of Cancer*, 105:1210–1217, 2011.
- [4] J. H. Lee, Mookwang Kwon, Woo Young Lim, Chae Rin Yoo, Y. Yoon, Dasol Han, Jin-Hyun Ahn, and K. Yoon. Yap inhibits hcmv replication by impairing sting-mediated nuclear transport of the viral genome. *PLOS Pathogens*, 18, 2022.
- [5] Shaoliang Li, Chisei Shimono, N. Norioka, Itsuko Nakano, Tetsuo Okubo, Y. Yagi, Maria Hayashi, Yuya Sato, H. Fujisaki, S. Hattori, N. Sugiura, K. Kimata, and K. Sekiguchi. Activin a binds to perlecan through its pro-region that has heparin/heparan sulfate binding activity\*. *The Journal of Biological Chemistry*, 285:36645 – 36655, 2010.
- [6] K. Maeshima, A. Maeshima, Y. Hayashi, S. Kishi, and I. Kojima. Crucial role of activin a in tubulogenesis of endothelial cells induced by vascular endothelial growth factor. *Endocrinology*, 145:3739–3745, 2004.
- [7] A. Maniotis, Xue Chen, Christopher Garcia, P. Dechristopher, Ding Wu, J. Pe'er, and R. Folberg. Control of melanoma morphogenesis, endothelial survival, and perfusion by extracellular matrix. *Laboratory Investigation*, 82:1031–1043, 2002.
- [8] D. McDonald and P. Baluk. Significance of blood vessel leakiness in cancer. *Cancer research*, 62 18:5381–5, 2002.
- [9] K.J. Murphy, D.A. Reed, C.R. Chambers, J. Zhu, A. Magenau, B.A. Pereira, P. Timpson, and D. Herrmann. Cell-derived matrix assays to assess extracellular matrix architecture and track cell movement. *Bio Protoc*, 12(24):e4570, Dec 2022.
- [10] KJ Murphy, DA Reed, CR Chambers, J Zhu, A Magenau, BA Pereira, P Timpson, and D Herrmann. Activin a-mediated polarization of cancer-associated fibroblasts and macrophages confers resistance to checkpoint immunotherapy in skin cancer. *Clinical Cancer Research*, 29:1942–1955, 2023.
- [11] Katarina Pinjusic, O. Dubey, O. Egorova, S. Nassiri, Etienne Meylan, julien Faget, and D. Constam. Inhibition of antitumor immunity by melanoma cell-derived activin-a depends on sting pathway activity. *Journal of Experimental Medicine*, 221:e20232145, 2024.
- [12] Seng-Ryong Woo, M. Fuertes, L. Corrales, S. Spranger, Michael J. Furdyna, M. Leung, Ryan Duggan, Ying Wang, G. Barber, K. Fitzgerald, M. Alegre, and T. Gajewski. Sting-dependent cytosolic dna sensing mediates innate immune recognition of immunogenic tumors. *Immunity*, 41 5:830–42, 2014.